Am J Physiol Cell Physiol 306: C607–C620, 2014.
First published January 22, 2014; doi:10.1152/ajpcell.00122.2013.

Force-dependent vinculin binding to talin in live cells: a crucial step in anchoring the actin cytoskeleton to focal adhesions

Hiroaki Hirata,[1,2] Hitoshi Tatsumi,[3] Chwee Teck Lim,[1,4] and Masahiro Sokabe[1,2,3]

[1]*Mechanobiology Institute, National University of Singapore, Singapore;* [2]*Cell Mechanosensing Project, International Cooperative Research Project/Solution-Oriented Research for Science and Technology, Japan Science and Technology Agency, Nagoya, Japan;* [3]*Department of Physiology, Nagoya University Graduate School of Medicine, Nagoya, Japan; and* [4]*Department of Biomedical Engineering and Department of Mechanical Engineering, National University of Singapore, Singapore*

Submitted 3 May 2013; accepted in final form 19 January 2014

Hirata H, Tatsumi H, Lim CT, Sokabe M. Force-dependent vinculin binding to talin in live cells: a crucial step in anchoring the actin cytoskeleton to focal adhesions. *Am J Physiol Cell Physiol* 306: C607–C620, 2014. First published January 22, 2014; doi:10.1152/ajpcell.00122.2013.—Mechanical forces play a pivotal role in the regulation of focal adhesions (FAs) where the actin cytoskeleton is anchored to the extracellular matrix through integrin and a variety of linker proteins including talin and vinculin. The localization of vinculin at FAs depends on mechanical forces. While in vitro studies have demonstrated the force-induced increase in vinculin binding to talin, it remains unclear whether such a mechanism exists at FAs in vivo. In this study, using fibroblasts cultured on elastic silicone substrata, we have examined the role of forces in modulating talin-vinculin binding at FAs. Stretching the substrata caused vinculin accumulation at talin-containing FAs, and this accumulation was abrogated by expressing the talin-binding domain of vinculin (domain D1, which inhibits endogenous vinculin from binding to talin). These results indicate that mechanical forces loaded to FAs facilitate vinculin binding to talin at FAs. In cell-protruding regions, the actin network moved backward over talin-containing FAs in domain D1-expressing cells while it was anchored to FAs in control cells, suggesting that the force-dependent vinculin binding to talin is crucial for anchoring the actin cytoskeleton to FAs in living cells.

talin; vinculin; focal adhesion; mechanotransduction; molecular clutch

CELL ADHESION TO EXTRACELLULAR matrices (ECMs) is crucial for cellular morphogenesis, migration, proliferation, and differentiation. Cell-to-ECM adhesion is primarily mediated by the transmembrane ECM receptors integrins. Integrin molecules are clustered at focal adhesions (FAs), where the actin cytoskeleton is anchored to the ECM through integrin clusters and plaques of a variety of linker proteins (16). There is bidirectional transmission of forces at FAs between ECM and the actin cytoskeleton (30). Thus FAs sustain tensile stress generated in the actin cytoskeleton. When integrin-actin cytoskeleton linkage is dissected, actin stress fibers are retracted and FAs are disassembled (37, 43, 53, 54), indicating that the linkage is crucial for maintaining the integrity of FAs.

Molecular processes of formation of integrin-cytoskeleton linkages have been extensively studied. Talin has both β-integrin- and actin-binding sites (9) and initially forms a molecular bond between ECM-bound integrin and the actin cytoskeleton in fibroblasts (17, 34, 65). The talin-mediated link between the actin cytoskeleton and clustered integrin is broken repeatedly by a small force of ~2 pN generated by the retrograde flow of actin filaments (34). On the other hand, the integrin-actin cytoskeleton linkage is strengthened when a mechanical force is loaded to it (7, 61). The strengthened linkage can sustain much larger forces (~20 pN), which prevents the slippage between the actin cytoskeleton and integrin clusters (7).

Vinculin also plays an important role in mediating the integrin-actin linkage because vinculin-deficient cells exhibit weaker linkage (1, 11). Vinculin binds to talin via its NH_2-terminal domain D1, while its COOH-terminal tail domain has an actin-binding site (19, 32, 66). Talin has up to 11 vinculin-binding sites (VBSs) in its rod domain (20). Some of the VBSs are buried in the bundles of amphipathic helices (12, 49) and are biochemically inactive in the native form (49, 51). However, molecular dynamics simulations have predicted that mechanical forces can expose such cryptic VBSs in the talin rod domain (29, 42). Indeed, application of a force to a single talin rod domain increases the number of vinculin head domains bound to the rod in vitro (10).

Vinculin localizes poorly at FAs in talin-deficient cells (17, 65), and the talin-binding domain of vinculin (domain D1) is localized at FAs when expressed ectopically (6, 27). These observations suggest that vinculin binds to talin at FAs. The effect of forces on the localization of talin and vinculin has also been examined. A reduction in the actomyosin-based force at FAs decreases the amount of vinculin at FAs (3), whereas external forces applied to FAs induce accumulation of vinculin at FAs (14, 55). This suggests that vinculin is localized to FAs in a force-dependent manner. In contrast to vinculin, the localization of talin at FAs is not affected by actomyosin-based forces (25, 40, 50).

These previous results support a model in which the force exerted on talin-containing FAs exposes the VBSs in talin, which facilitates vinculin localization at FAs and strengthens the linkage between integrin and the actin cytoskeleton (47). However, it has not been tested whether the talin-vinculin binding at FAs is really modulated by mechanical forces in living cells, and the role of this binding in the integrin-actin cytoskeleton linkage has not been explored in detail. In this study, we examined whether *1*) the mechanical force applied on FAs increases the amount of vinculin bound to talin at FAs, and *2*) the talin-vinculin binding strengthens the integrin-actin cytoskeleton linkage at FAs. Human foreskin fibroblasts, which have been used for studies on force-dependent regula-

Address for reprint requests and other correspondence: M. Sokabe, Dept. of Physiology, Nagoya Univ. Graduate School of Medicine, 65 Tsurumai, Showa-ku, Nagoya, Aichi 466-8550, Japan (e-mail: msokabe@med.nagoya-u.ac.jp).

tions of FAs (3, 25, 35), were cultured on elastic silicone substrata, and mechanical forces were applied to FAs by stretching the substrata. Our results showed that the tensile force on the actin-talin-integrin linkage facilitates the talin-vinculin binding at FAs, which could be a critical step in strengthening the linkage between the actin cytoskeleton and integrins.

MATERIALS AND METHODS

Cell culture. Human foreskin fibroblasts (HFFs) and HeLa cells were cultured in Dulbecco's modified Eagle's medium (Sigma Chemical, St. Louis, MO) supplemented with 10% fetal bovine serum (Nipro, Osaka, Japan) at 37°C in 5% CO_2. For immunofluorescence experiments, HFF cells were grown for 15 h on glass coverslips or elastic silicone (polydimethylsiloxane elastomer) chambers (Strex, Osaka, Japan), which were precoated with 100 μg/ml fibronectin (Sigma Chemical). In some cases, cells were treated with 100 μM blebbistatin (Toronto Research Chemicals, North York, Canada) or 40 μM Y-27632 (Calbiochem, San Diego, CA) for 30 min.

Antibodies. Mouse anti-vinculin and -β-actin mAbs were purchased from Sigma Chemical. Mouse anti-talin mAbs were from Sigma Chemical and Chemicon (Temecula, CA). The rabbit anti-α_5-integrin polyclonal antibody was from Chemicon. The mouse anti-$\alpha_5\beta_1$-integrin mAb was from Millipore (Billerica, MA). The mouse anti-green fluorescent protein (GFP) mAb was from Clontech Laboratories (Mountain View, CA). Control mouse IgG1 was from R&D Systems (Minneapolis, MN). Alexa488-chicken anti-rabbit IgG, Alexa546-goat anti-mouse IgG, and Alexa594-chicken anti-rabbit IgG antibodies, and Alexa488- and Alexa647-phalloidin were from Molecular Probes (Eugene, OR). Horseradish peroxidase-conjugated anti-mouse IgG antibody was from GE Healthcare (Little Chalfont, UK). Horseradish peroxidase-conjugated Mouse TrueBlot ULTRA was from eBioscience (San Diego, CA). The anti-vinculin mAb hVIN-1 recognizes full-length vinculin, but not the vinculin domain D1, in immunoblot (data not shown).

Plasmids and transfection. The vinculin domain D1 (amino acid 1–258) (19, 32) was amplified by PCR using mouse vinculin cDNA (a gift from Cheng-Han Yu, National University of Singapore) (64) as a template and subcloned into the pcDNA3-EGFP vector. The A50I mutant form of the domain D1 was generated by the QuickChange mutagenesis method (Agilent Technologies, Santa Clara, CA) using primers 5′-CGCCGTGCAGGCGATCGTCAGCAACCTCGTC-3′ and 5′-GACGAGGTTGCTGACGATCGCCTGCACGGCG-3′. pcDNA3-EGFP and pcDNA3-α-actinin-1-mCherry were provided by Hiroaki Machiyama (National University of Singapore).

For introducing EGFP, EGFP-D1, EGFP-vinculin, and/or α-actinin-mCherry into HFF cells, cells were transiently transfected with their expression plasmids using the Lipofectamine 2000 transfection reagent (Invitrogen, Carlsbad, CA) according to the manufacturer's instruction.

Fluorescence microscopy and image analysis. For immunofluorescence, cells were fixed and permeabilized for 30 min with 4% formaldehyde and 0.2% Triton X-100 in cytoskeleton stabilizing buffer (137 mM NaCl, 5 mM KCl, 1.1 mM Na_2HPO_4, 0.4 mM KH_2PO_4, 4 mM $NaHCO_3$, 2 mM $MgCl_2$, 5.5 mM glucose, 2 mM EGTA, and 5 mM PIPES pH 6.1) (8). This was followed by blocking with 1% skim milk (Becton-Dickinson, Franklin Lakes, NJ) in cytoskeleton stabilizing buffer for 30 min. The cells were then incubated with primary antibodies for 40 min, washed, and further incubated with secondary antibodies for 40 min. Antibodies were diluted to 1:100 in cytoskeleton stabilizing buffer containing 1% skim milk.

For live cell imaging, cells were observed in cell culture medium at 37°C in 5% CO_2. The cells were observed with an epifluorescence inverted microscope (IX81; Olympus, Tokyo, Japan) equipped with an oil immersion objective (NA 1.45, ×100; PlanApo; Olympus) and a charge-coupled device camera (CoolSNAP EZ; Photometrics, Tucson, AZ). The Metamorph software (Molecular Devices, Sunnyvale, CA) was used for image acquisition. Acquired images were analyzed offline using the public domain software ImageJ (version 1.45f).

Fluorescence intensities of proteins at FAs were analyzed as follows: all FAs were included for quantitative analyses except those in the perinuclear area of which the background fluorescence intensity was too high to perform precise measurements (data not shown). The area of each FA was determined by counting the number of pixels where fluorescence intensity was higher than the half maximum fluorescence intensity of the FA. The mean fluorescence intensities of FA proteins in the FAs were calculated for each cell and used for ratiometric and correlation analyses. The ratio of the mean value of vinculin (or talin) against that of α_5-integrin was then calculated. The correlation analysis of fluorescence intensities of two different proteins at FAs was carried out by plotting the mean value of one protein against the mean value of the other (see Fig. 3). Cells highly expressing GFP-fused proteins were excluded from fluorescence intensity analyses because cells expressing GFP-D1 at the extremely high level were less well spread, and talin clusters did not show the typical elongated shapes (data not shown) compared with control cells.

Kymographs were generated along lines placed in the direction of retrograde actin movement in protruding regions of cells. The velocity of actin cytoskeletal movement was calculated from these kymographs. Protrusion velocity was obtained from displacement of the leading edge for 10 min.

Stretching-cell assay. Stretching-cell assays were performed as described previously (25). In brief, cells grown on an elastic silicone chamber were first treated with 100 μM blebbistatin for 30 min and then uniaxially stretched by 50% for 3 min in the presence of blebbistatin. When indicated, 10 μM cytochalasin D (Sigma Chemical) or DMSO were also added to the medium. The stretched cells were used for immunofluorescence staining or immunoblotting. Vinculin accumulation at FAs was regained in ~80% of blebbistatin-treated cells upon 40–50% stretch. However, only <10% of blebbistatin-treated cells showed vinculin accumulation at FAs after 20% stretch, suggesting that a high magnitude of stretch was needed for vinculin accumulation under the condition where the basal level of tension was dropped by the myosin II inhibition.

Immunoblot. Cells were lysed with 2× lithium dodecyl sulfate sample buffer (Invitrogen) containing 2.5% β-mercaptoethanol. The lysate samples were resolved by SDS-PAGE (4–12% Bis-Tris gel; Invitrogen), transferred onto a polyvinylidene fluoride membrane (Millipore), and probed with antibodies. Immunoreactive bands were detected with SuperSignal West Pico Chemiluminescent Substrate (Thermo Fisher Scientific, Rockford, IL).

Protein cross-linking and immunoprecipitation. The anti-talin mAb (Chemicon) and control mouse IgG1 were covalently coupled to protein G-conjugated magnetic beads (Invitrogen) with 20 mM dimethyl pimelimidate·2 HCl (Thermo Fisher Scientific, Rockford, IL) according to the manufacturer's instruction.

HFF or HeLa cells were grown for 15 h on either 10-cm tissue culture plates or 2 × 2 cm elastic silicone chambers, which were pretreated with 40 μM Y-27632 or DMSO (control) for 30 min if needed. Since the efficiency of DNA transfection into HFF cells is too low (~20%), highly transfectable HeLa cells, whose transfection efficiency was >90%, were used for the immunoprecipitation (IP) experiments following DNA transfection. The silicone chambers were subjected to a uniaxial 50% stretch for 3 min in the presence of Y-27632, when indicated. The cells were washed three times with warmed (ca. 37°C) standard external solution (SES; 140 mM NaCl, 5 mM KCl, 1.8 mM $CaCl_2$, 0.8 mM $MgCl_2$, 10 mM glucose, and 10 mM HEPES, pH 7.4) and then incubated for 30 min at 37°C with 0.5 mM dithiobis[succinimidyl propionate] (DSP; Thermo Fisher Scientific), a membrane-permeable and thiol-cleavable NHS-ester cross-linker, or DMSO in SES in the presence or the absence of 40 μM Y-27632. The DSP concentration used here (i.e., 0.5 mM) was in

the same range used in previous IP experiments of cell adhesion-related proteins (28, 41, 56). Cross-linking reactions were quenched with 1% glycine in cold SES for 15 min on ice. After being washed twice with cold SES, cells were lysed with the lysis buffer (1% NP-40, 150 mM NaCl, 20 mM Tris, and 1 mM EDTA pH 8.0) supplemented with the protease inhibitor cocktail (Sigma Chemical). The cell lysates were incubated for 30 min on ice and then centrifuged for 40 min at 20,000 *g*. The protein concentration in the supernatants was measured with the bicinchoninic acid (BCA) method (Thermo Fisher Scientific), and the concentration was equalized among samples by adding the lysis buffer. The concentration-adjusted supernatants were incubated with antibody-coupled magnetic beads overnight at 4°C. The beads were washed three times with the lysis buffer, and then, the precipitated proteins were eluted with 2× lithium dodecyl sulfate sample buffer (Invitrogen) containing 2.5% β-mercaptoethanol. IP samples were subjected to immunoblot analyses using horseradish peroxidase-conjugated Mouse TrueBlot ULTRA as a secondary antibody.

Statistical analysis. Numerical results were presented as means ± SD. Statistical significance was assessed using Student's *t*-test.

RESULTS

Mechanical stretch of the cell substratum facilitates the binding of vinculin to talin at FAs. Mechanical forces were applied to FAs by stretching fibronectin (FN)-coated elastic substrata to which HFF cells adhered. Cells were treated with the myosin II inhibitor blebbistatin (57) to eliminate the basal effect of actomyosin-generated forces. Vinculin was delocalized from FAs upon treating cells with either blebbistatin or the Rho kinase inhibitor Y-27632 (59) as reported previously (25, 40, 50), whereas talin and α_5-integrin were retained at FAs (Fig. 1). In these cells, retained α_5-integrin presumably forms a heterodimer with β_1-integrin and binds to FN at FAs (24, 25).

Vinculin was reaccumulated at FAs in blebbistatin-treated cells when subjected to sustained uniaxial stretching (50% stretch for 3 min) (Fig. 2, *A*, *B*, and *D*). By contrast, the distribution of neither talin nor α_5-integrin was affected (Fig. 2, *C* and *E*). Since inhibition of actomyosin contractility declined basal tension in stress fibers (21, 25), relatively large stretch was required for reaccumulation of vinculin in blebbistatin-treated cells.

To examine the role of talin-vinculin binding in vinculin accumulation at FAs, this binding was impaired by expressing the talin-binding domain of vinculin (domain D1) (19, 32), and the distribution of vinculin and talin was analyzed. The GFP-tagged domain D1 (GFP-D1) was colocalized with talin at FAs when expressed in HFF cells (Fig. 3, *A* and *B*), which is consistent with the previous reports (6, 27). The current study showed, for the first time, that endogenous vinculin was delocalized from FAs in GFP-D1-expressing cells (Fig. 3*C*); the fluorescence intensity of endogenous vinculin at FAs was negatively correlated with that of GFP-D1 (Fig. 3, *D* and *E*). To check whether GFP-D1 interferes specifically with the talin-vinculin binding, we examined the action of the A50I mutant form of D1 ($D1_{A50I}$) on the localization of endogenous vinculin at FAs, because the vinculin binding to talin is impaired by the A50I mutation in vinculin in vitro (2). GFP-$D1_{A50I}$ was scarcely accumulated at FAs compared with GFP-D1 (Fig. 3*C*) and did not displace endogenous vinculin from FAs as effectively as GFP-D1 did (Fig. 3, *C-E*), suggesting that the interfering action of GFP-D1 on endogenous vinculin was virtually specific. It is important to note that talin accumulation at FAs was not affected by expression of GFP-D1 or GFP-$D1_{A50I}$ (Fig. 3*E* and data not shown). These results indicate that localization of vinculin at FAs is mediated by the talin-vinculin interaction via the domain D1 and GFP-D1 acts as a dominant negative form of vinculin to interfere with the talin-vinculin binding in cells.

Binding of α-actinin to the domain D1 of vinculin in vitro has been reported (4, 36). In our experimental condition, however, GFP-D1 did not apparently colocalize with α-actinin (Fig. 3*F*), suggesting that GFP-D1 does not interfere with the interaction between endogenous vinculin and α-actinin at FAs in vivo.

Cells expressing high levels of GFP-D1 were spread poorly, and talin clusters in these cells showed abnormal shapes (data not shown), whereas cells expressing GFP-$D1_{A50I}$ or GFP were normal in morphology and had talin clusters with typical elongated shapes. These suggest that the talin-vinculin interaction plays a crucial role in cell spreading and protein assembly at FAs.

GFP-D1 was localized at FAs in actomyosin-inhibited cells as reported previously (6, 27), and the pattern of the localization was not affected by uniaxial stretching of these cells (Fig. 4*A*). On the other hand, stretch-induced accumulation of endogenous vinculin to FAs was abrogated in GFP-D1-expressing cells, whereas the accumulation was seen in control cells expressing GFP (Fig. 4*B*). These results reveal that talin-vinculin interaction is responsible for the stretch-induced vinculin accumulation at FAs and strongly suggest that the mechanical force loaded to FAs facilitates the binding of vinculin to talin at FAs.

Connection of stress fiber-like structures to FAs is required for the stretch-dependent vinculin accumulation at FAs. Actin stress fibers are crucial for force transmission and mechanotransduction at FAs (23, 25, 39, 43); stress fibers may transmit forces to the talin-integrin-FN complexes thereby enhancing the binding of vinculin to talin. The distribution of stretch-dependent vinculin accumulation at FAs and the pattern of stress fiber-like structures were examined in blebbistatin-treated cells, where a small fraction of stress fiber-like structures were retained even after the drug treatment (Fig. 5*A*, yellow arrows). Stretching caused vinculin accumulation at not all of the FAs but only those associated with stress fiber-like structures (Fig. 5, *A* and *B*). This was confirmed by analyzing the fluorescence intensity profiles of α_5-integrin, vinculin, and F-actin (Fig. 5*C*). By contrast, talin was accumulated at FAs regardless of the presence or absence of stress fiber-like structures associated with FAs (Fig. 5, *B* and *D*). When the actin cytoskeleton was disrupted by treating cells with cytochalasin D, the stretch-induced vinculin accumulation at FAs was almost abolished (Fig. 5, *E* and *F*), while talin localization at FAs was not affected (Fig. 5F and data not shown). The correlations presented in Fig. 5 do not address the direct interaction between talin and vinculin. However, together with the results using D1 and $D1_{A50I}$ domains in the above and following sections, our observations support the idea that force-dependent direct interaction between talin and vinculin is crucial for the stretch-induced accumulation of vinculin at talin-containing FAs.

The width of vinculin or talin accumulations in the stretched cells was often wider than that of the associated actin bundle (e.g., the *rightmost 2 peaks* indicated by filled arrows in Fig. 5*C*, and the *leftmost peak* indicated by a filled arrow in Fig.

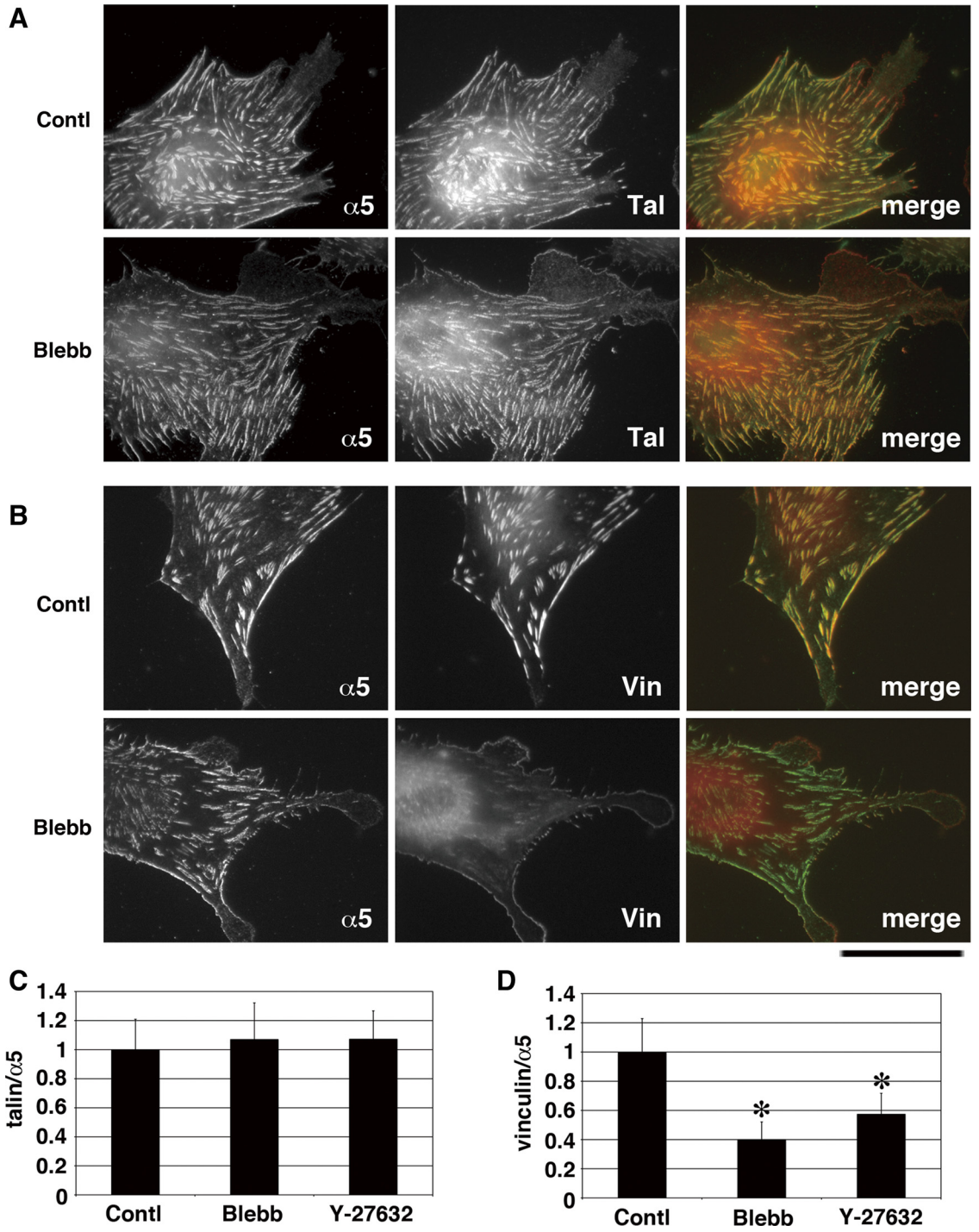

Fig. 1. Delocalization of vinculin, but not talin, from focal adhesions (FAs) upon inhibition of myosin II. *A* and *B*: human foreskin fibroblasts (HFFs) cells were treated without (Contl) or with 100 μM blebbistatin for 30 min (Blebb) and then double-stained for α_5-integrin (α_5) and either talin (Tal; *A*) or vinculin (Vin; *B*). Merged images (green for α_5-integrin and red for vinculin or talin) are also shown. Bar = 50 μm. *C* and *D*: fluorescence intensity ratio of talin (*C*) or vinculin (*D*) against α_5-integrin at FAs in control (Contl), blebbistatin-treated (Blebb), or Y-27632-treated (Y-27632) cells. Values were normalized with respect to the mean values of control cells. Fluorescence images of Y-27632-treated cells, which were nearly the same as those of blebbistatin-treated ones, were not shown. Each bar represents the mean s± SD for >30 cells. *$P < 0.001$ (unpaired *t*-test).

5*D*); however, the underlying mechanism is not apparent at present.

The modified immunoprecipitation assay suggests force-dependent talin-vinculin complex formation. We conducted IP experiments to test whether the talin-vinculin complex formation was force dependent in cells. The effect of actomyosin inhibition on talin-vinculin complex formation was not detected using a conventional IP method (50); presumably the protein complexes became unstable in cell lysates since actomyosin-dependent forces would no longer be loaded to these pro-

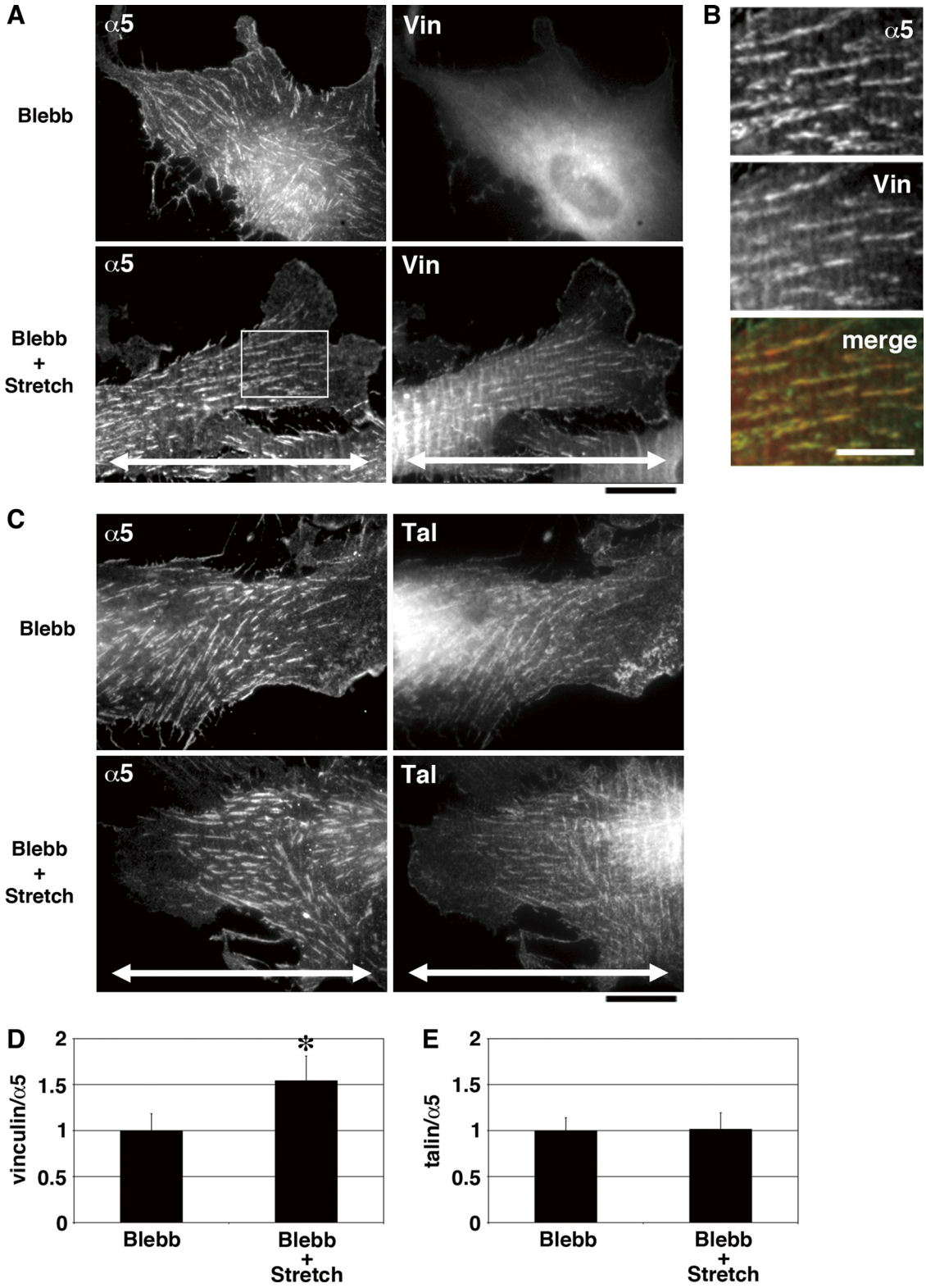

Fig. 2. Stretching substrata induces vinculin accumulation at FAs but do not affect talin localization at FAs in myosin II-inhibited cells. *A–C*: HFF cells grown on fibronectin (FN)-coated elastic substrata were treated with 100 μM blebbistatin for 30 min, and then the substrata were uniaxially stretched (50% for 3 min) in the presence of blebbistatin. Cells without (Blebb) or with stretching substratum (Blebb + Stretch) were double-stained for α_5-integrin (α5) and either vinculin (Vin) or talin (Tal). Double-headed arrows indicate the direction of the stretch axis. *B*: high magnification of the boxed area in *A*. Merged image (green for α_5-integrin and red for vinculin) is also shown. Bars = 20 μm in *A* and *C* and 10 μm in *B*. *D* and *E*: fluorescence intensity ratio of vinculin (*D*) or talin (*E*) against α_5-integrin at FAs in blebbistatin-treated cells without (Blebb) or with stretching substratum (Blebb + Stretch). Values were normalized with respect to the mean values of cells without stretching. Each bar represents the means ± SD for >18 cells. $^*P < 0.001$ (unpaired *t*-test).

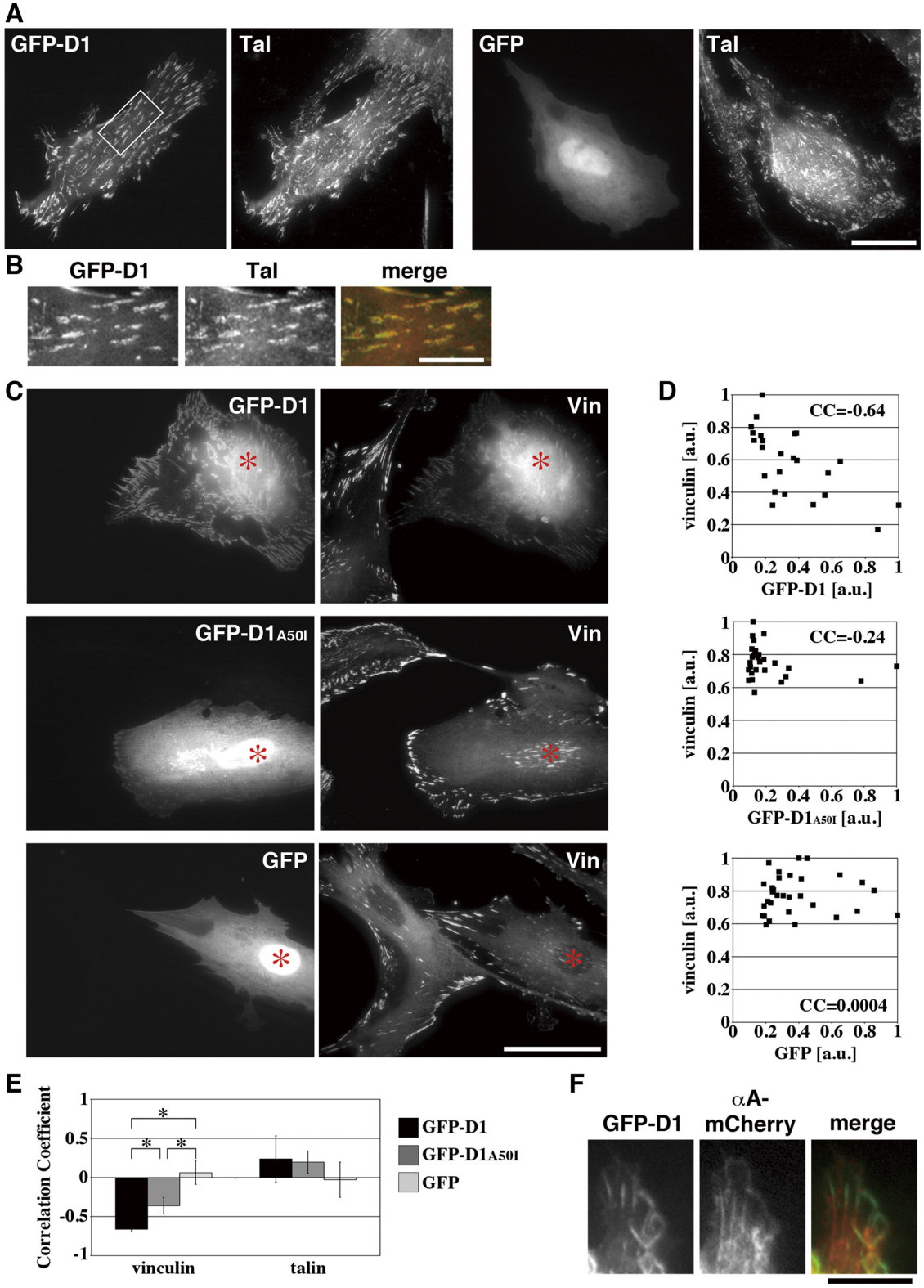

Fig. 3. Green fluorescent protein (GFP)-D1 acts as a dominant-negative form against talin-vinculin binding at FAs. *A*: HFF cells grown on FN were transfected with GFP-D1 or GFP and then stained for talin (Tal). *B*: high magnification of the boxed area in *A*. Merged image (green for GFP-D1 and red for talin) is also shown. *C*: HFF cells were transfected with GFP-D1, GFP-D1$_{A50I}$ or GFP, and then stained for endogenous vinculin (Vin). *Cells expressing the exogenous molecules. *D*: averaged fluorescence intensity of endogenous vinculin at FAs was plotted against that of GFP-D1, GFP-D1$_{A50I}$, or GFP for each cell. Values were normalized with respect to the maximum value on each axis. CC, correlation coefficient. *E*: correlation coefficients of averaged fluorescence intensities of endogenous vinculin vs. GFP-D1 (black bars), GFP-D1$_{A50I}$ (dark gray bars) or GFP (light gray bars). Correlation coefficients of talin vs. the same series of GFP-tagged proteins are also shown. Each bar represents the mean ± SD for 3 independent experiments. *$P < 0.05$ (unpaired *t*-test). *F*: HFF cells grown on FN were cotransfected with GFP-D1 and α-actinin (αA)-mCherry. Merged image (green for GFP-D1 and red for αA-mCherry) is also shown. Bars = 50 μm in *A* and *C* and 20 μm in *B* and *F*.

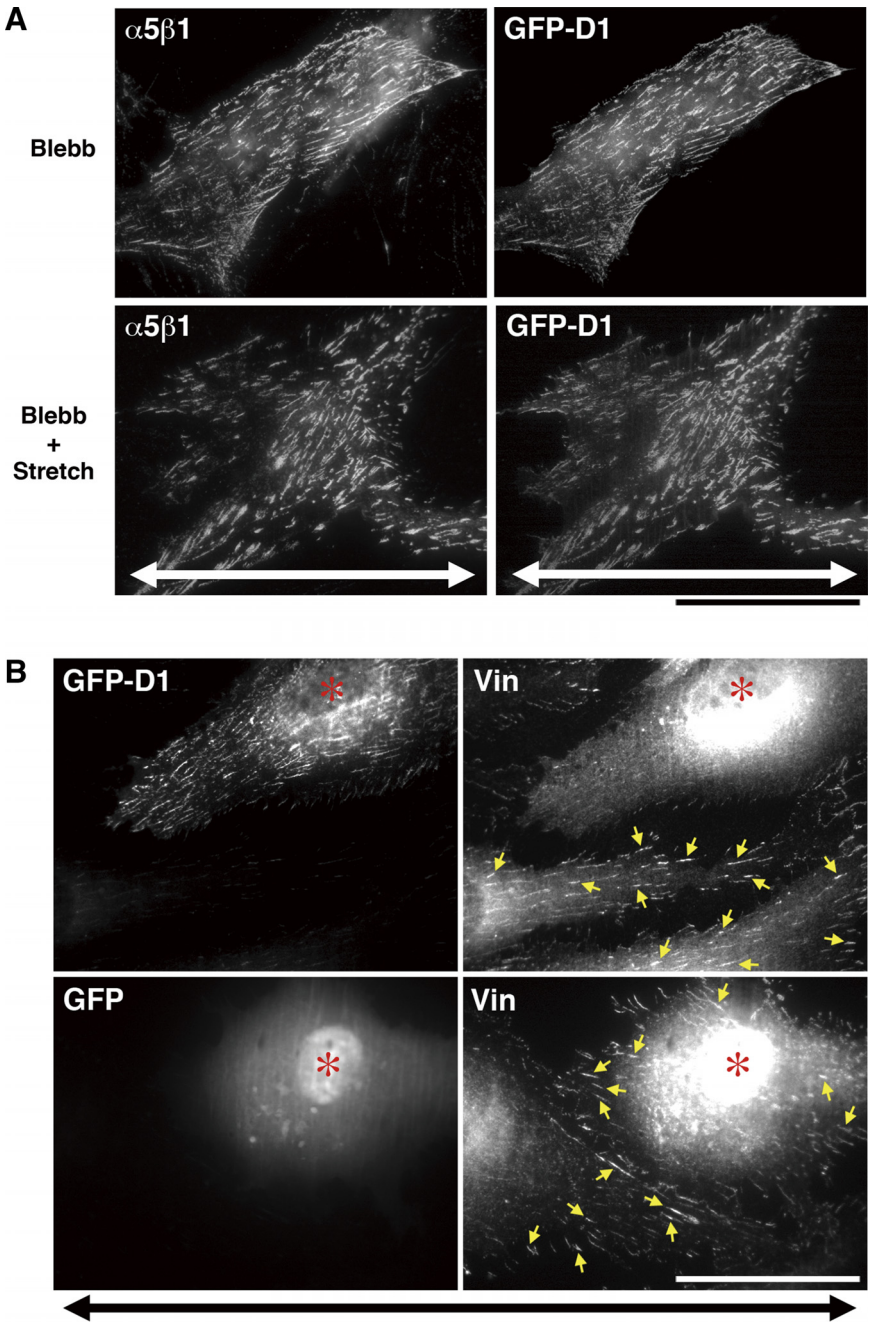

Fig. 4. Inhibition of talin-vinculin binding abrogates the stretch-induced vinculin accumulation at FAs. *A*: HFF cells grown on FN-coated elastic substrata and transfected with GFP-D1 were treated with 100 μM blebbistatin for 30 min, and then the substrata were uniaxially stretched (50% for 3 min) in the presence of blebbistatin. Cells without (Blebb) or with stretching substratum (Blebb + Stretch) were stained for $\alpha_5\beta_1$-integrin. *B*: HFF cells grown on FN-coated elastic substrata were transfected with GFP-D1 or GFP and treated with 100 μM blebbistatin for 30 min. The substrata were uniaxially stretched (50% for 3 min) in the presence of blebbistatin, and cells were stained for endogenous vinculin (Vin). *Cells expressing GFP-D1 or GFP. Yellow arrows indicate vinculin accumulations. Double-headed arrows indicate the direction of the stretch axis. Bars = 50 μm.

teins, and the protein complexes that require forces to keep them together would be dissociated during the IP procedures. To prevent the disassembly, cells were treated with the membrane-permeable cross-linker DSP before the lysis for IP.

Talin was precipitated with the anti-talin antibody; however, the amount of precipitated talin was reduced in the DSP-cross-linked cell lysate compared with that in the non-cross-linked one (Fig. 6*A*). One possible explanation of this is that the DSP treatment may modulate the epitope recognition of the anti-talin antibody. The amount of vinculin coprecipitated with talin from the cross-linked lysate was larger than that from the non-cross-linked lysate (Fig. 6, *A* and *B*), implying that certain fraction of vinculin-talin complexes were cross-linked and preserved during IP.

Coprecipitation of vinculin with talin from the cross-linked lysate might be mediated through cross-linking these proteins to a third protein(s), e.g., actin; the coprecipitation of vinculin with talin might be indirect. To test the direct interaction between talin and vinculin, the lysate from GFP-D1-expressing cells was used for IP, which interferes with the binding. Expression of GFP-D1, but not GFP-D1$_{A50I}$, significantly decreased the amount of vinculin coprecipitated with talin (Fig. 6, *C* and *D*), suggesting that the talin-vinculin direct interaction substantially mediates the vinculin coprecipitation.

Cells were treated with Y-27632 before and during the protein-cross-linking to examine the effect of actomyosin inhibition on the amount of talin-vinculin complexes in living cells. The yield of vinculin coprecipitated with talin

and the ratio of precipitated vinculin against talin were significantly decreased by Y-27632 treatment (Fig. 6, *A* and *B*), indicating that the talin-vinculin complex formation depends on the actomyosin activity. The effect of stretching of the cell substrata on the talin-vinculin complex was also examined; the ratio of precipitated vinculin against talin was significantly increased when cells were exposed to the uniaxial stretching (Fig. 6, *E* and *F*). These IP results

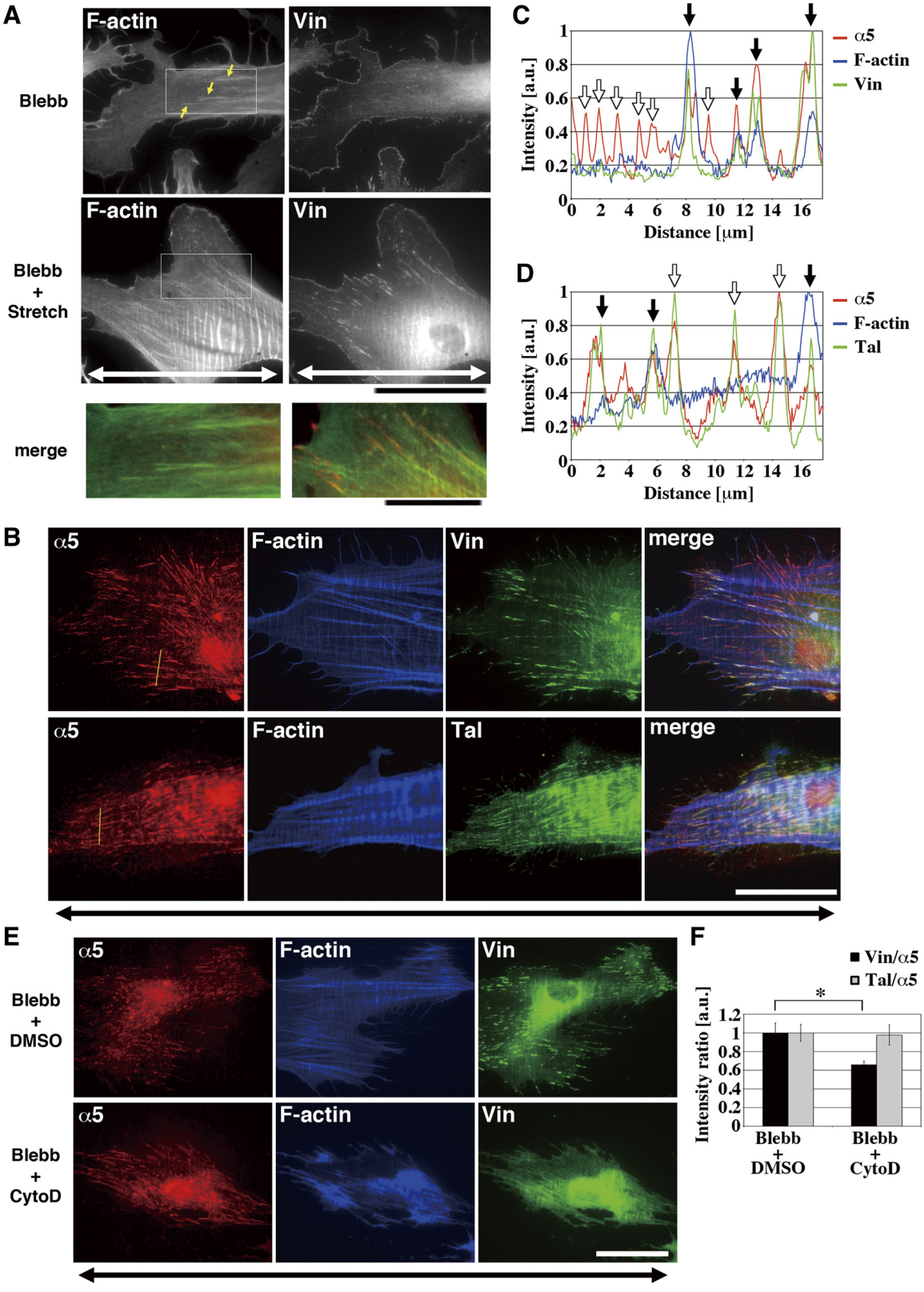

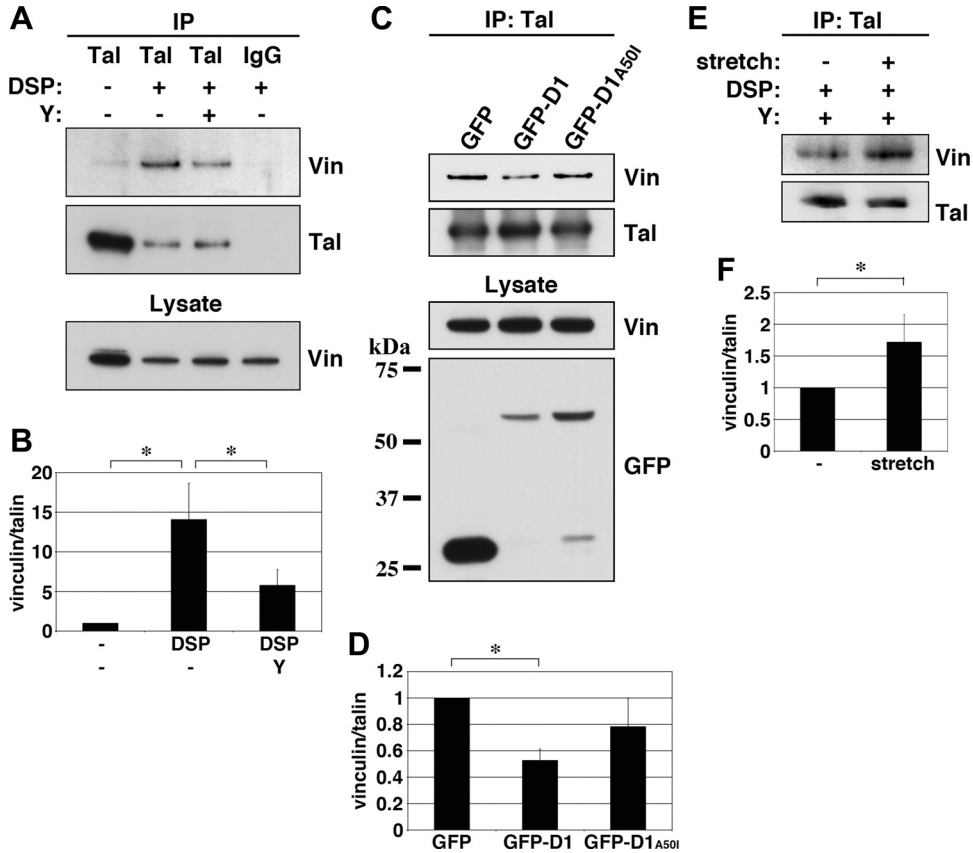

Fig. 6. The amount of talin-vinculin complex is force dependent. *A*: HFF cells treated with or without 40 μM Y-27632 (Y) were incubated with or without 0.5 mM DSP for 30 min to cross-link cellular proteins in the presence or the absence of 40 μM Y-27632. Lysates from these cells were subjected to immunoprecipitation (IP) with the anti-talin antibody (Tal) or control IgG and then immunoblotted for vinculin (Vin) and talin (Tal). The DSP-mediated cross-link was cleaved by reduction with 2.5% β-mercaptoethanol when the precipitated proteins were eluted with lithium dodecyl sulfate sample buffer. The level of vinculin was higher in non-cross-linked lysate and was declined in cross-linked ones, which could be in part due to some fraction of vinculin was partitioned together with F-actin into the insoluble fraction in cross-linked lysates. *B*: quantification of the densitometric ratio of precipitated vinculin against talin shown in *A*. Each bar represents the means ± SD for 4 independent experiments. *$P < 0.05$ (unpaired *t*-test). *C*: HeLa cells transfected with either GFP, GFP-D1, or GFP-D1$_{A50I}$ were incubated with 0.5 mM DSP for 30 min. Lysates from these cells were subjected to IP with the anti-talin antibody, and then immunoblotted for vinculin (Vin), talin (Tal), and GFP. *D*: quantification of the densitometric ratio of precipitated vinculin against talin shown in *C*. Each bar represents the means ± SD for 4 independent experiments. *$P < 0.01$ (unpaired *t*-test). *E*: HFF cells grown on FN-coated elastic substrata were treated with 40 μM Y-27632 for 30 min, and then the substrata were uniaxially stretched (50% for 3 min) in the presence of Y-27632. These cells under uniaxial stretch were treated with 0.5 mM DSP for 30 min in the presence of 40 μM Y-27632 (Y). Lysates from the cells with or without stretching were subjected to IP with the anti-talin antibody and immunoblotted for vinculin (Vin) and talin (Tal). *F*: quantification of the densitometric ratio of precipitated vinculin against talin shown in *E*. Each bar represents the means ± SD for 3 independent experiments. *$P < 0.05$ (unpaired *t*-test).

suggest that the talin-vinculin complex formation in living cells is force dependent.

Talin-vinculin binding is essential for anchoring the actin network to FAs. Talin links the actin cytoskeleton to ECM-bound integrins, but this talin-mediated link is relatively weak and easily slips (34). On the other hand, the actin cytoskeleton is stably anchored to FAs containing talin in intact cells. The hypothesis that force-dependent vinculin

Fig. 5. Stress fiber-like structures connected to FAs are required for stretch-induced vinculin accumulation at FAs. *A* and *B*: HFF cells grown on FN-coated elastic substrata were treated with 100 μM blebbistatin for 30 min, and the substrata were uniaxially stretched (50% for 3 min) in the presence of blebbistatin. *A*: cells without (Blebb) or with stretching substratum (Blebb + Stretch) were double-stained for F-actin (F-actin) and vinculin (Vin). Double-headed arrows indicate the direction of the stretch axis. Magnified and merged images (green for F-actin and red for vinculin) of two boxed areas in *A* are also shown. *B*: cells with stretching substratum were triple-stained for α_5-integrin (α_5), F-actin (F-actin), and either vinculin (Vin) or talin (Tal). Merged images are also shown. Double-headed arrow indicates the direction of the stretch axis. Note that stretch-induced vinculin accumulation was observed virtually exclusively at FAs that were associated with actin bundles. Bars = 50 μm. *C* and *D*: fluorescence intensity profiles of α_5-integrin (α5; red line), F-actin (F-actin; blue line), and either vinculin (Vin; green line in *C*) or talin (Tal; green line in *D*) along two yellow lines in the α_5-integrin images of *B*. Values were normalized with respect to the maximum value in each profile. Filled arrows in *C* indicate α_5-integrin-labeled FAs where stress fiber-like structures are associated and vinculin is accumulated. Open arrows in *C* indicate FAs that are deficient in association with stress fiber-like structures. Filled and open arrows in *D*, respectively, indicate FAs with and without associated actin bundles, where talin is accumulated at α_5-integrin-labeled FAs regardless of their association with stress fiber-like structures. *E*: HFF cells grown on FN-coated elastic substrata were treated with 100 μM blebbistatin and either DMSO (Blebb + DMSO, control) or 10 μM cytochalasin D (Blebb + CytoD) for 30 min, and the substrata were uniaxially stretched (50% for 3 min). Cells were triple-stained for α_5-integrin (α5), F-actin (F-actin), and vinculin (Vin). Double-headed arrow indicates the direction of the stretch axis. Bar = 50 μm. *F*: fluorescence intensity ratio of vinculin (Vin/α5) or talin (Tal/α5) against α_5-integrin at FAs in cells that were treated with 100 μM blebbistatin and either DMSO (Blebb + DMSO, control) or 10 μM cytochalasin D (Blebb + CytoD) for 30 min and then uniaxially stretched (50% for 3 min). Values were normalized with respect to the mean values of control cells. Each bar represents the means ± SD for >30 cells. *$P < 0.001$ (unpaired *t*-test).

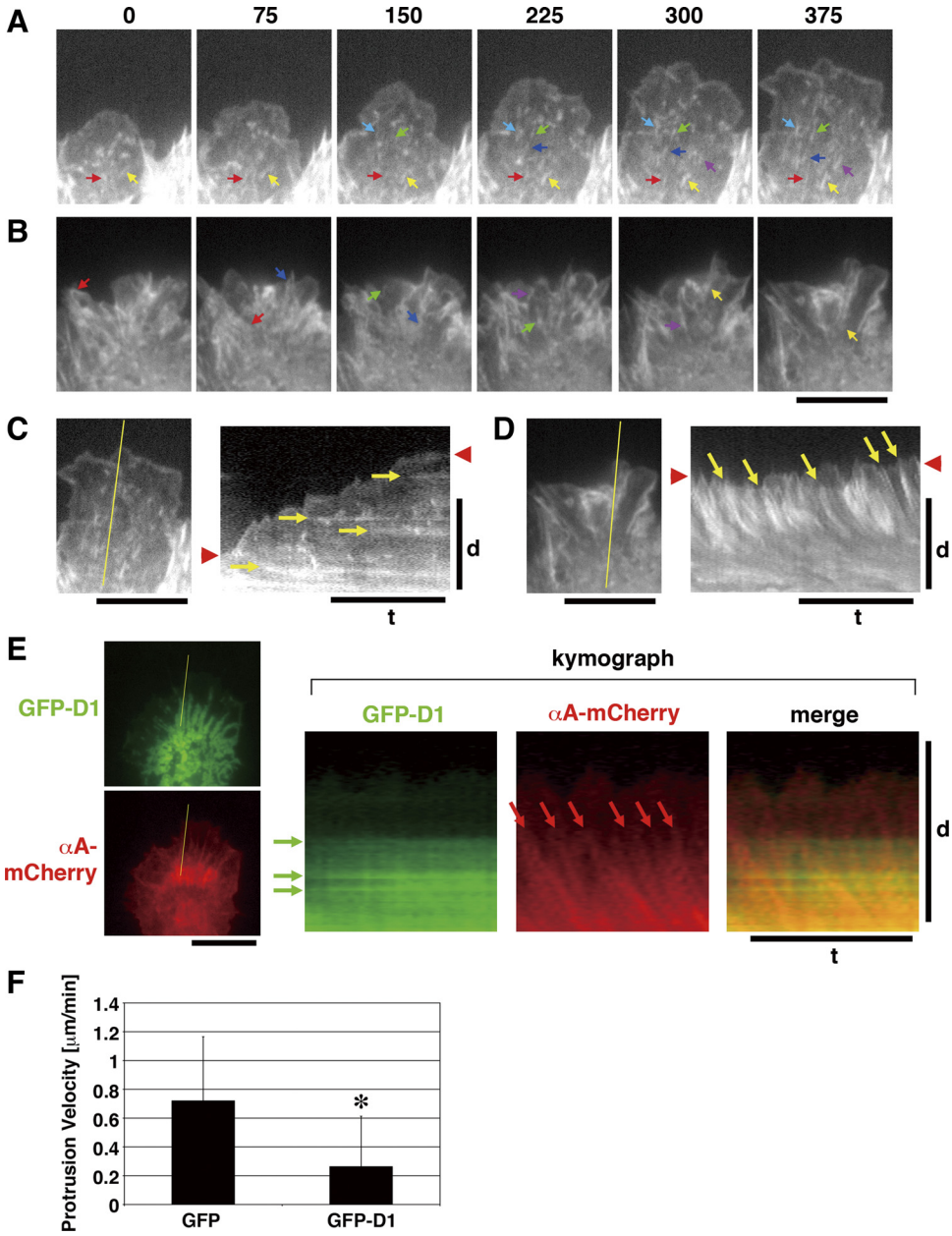

Fig. 7. Inhibition of talin-vinculin binding causes retrograde movement of the actin network over talin-localized FAs. HFF cells were cotransfected with α-actinin-mCherry and GFP (*A* and *C*) for control or α-actinin-mCherry and GFP-D1 (*B*, *D*, and *E*). *A* and *B*: time-lapse images of α-actinin-mCherry in a control cell (*A*) or in a GFP-D1-expressing cell (*B*). Individual α-actinin clusters were indicated by arrows with different colors. Elapsed time (in seconds) is shown above the panels. Bar = 10 μm. *C* and *D*: kymograph analyses of actin network movement. Kymographs (*right*) were generated along the yellow lines at *left*. Yellow arrows in the kymograph indicate horizontal lines showing stationary α-actinin clusters (*C*) or downward-sloping lines showing α-actinin clusters moving retrogradely (*D*). The red arrowheads denote initial and final positions of leading edges. Space bar (*left* and d in kymographs), 10 μm, and time bar (t in kymographs), 5 min. *E*, *leftmost 2 panels*: images of GFP-D1 (green) and α-actinin-mCherry (αA-mCherry, red) in a cell protruding region. Kymographs were generated along the yellow lines in the *leftmost panels*. The green arrows indicate horizontal lines corresponding to the GFP-D1 clusters staying at the same place, and the red arrows indicate downward-sloping lines showing α-actinin clusters moving in the retrograde direction. Kymograph merged with colors is also shown. Space bars (*the leftmost 2 panels* and d in kymographs) denote 10 μm, and the time bar (t in kymographs) 5 min. *F*: protrusion velocities of cells coexpressing α-actinin-mCherry and either GFP or GFP-D1. All protruding regions (19 protrusions found in 16 GFP-expressing cells, and 16 in 13 GFP-D1-expressing cells) in two independent sets of experiments were analyzed. Each bar represents the means ± SD. *$P < 0.005$ (two-tailed, unpaired *t*-test).

recruitment to the talin-integrin-FN complexes is involved in anchoring the actin cytoskeleton to FAs was examined by impairing the talin-vinculin binding and by observing the retrograde movement of the actin network in cell protruding regions because the velocity of retrograde actin movement is affected by mechanical connection between the actin cytoskeleton and FAs (15).

Dynamic movement of the actin network was observed using α-actinin-mCherry and analyzed. About 20–30% of cells coexpressing α-actinin-mCherry and either GFP-D1 or GFP had one or two protruding lamellae. Patches of α-actinin stayed in the same position in protruding regions of control cells expressing GFP (Fig. 7, *A* and *C*, arrows; Supplemental Movie S1; Supplemental Material for this article is available online at the *Am J Physiol Cell Physiol* website). By contrast, the actin network moved backward (Fig. 7, *B* and *D*, arrows; Supplemental Movie S1) at the rate of 3.8 ± 1.8 μm/min (means ± SD; $n = 16$ protruding regions) in α-actinin-mCherry/GFP-D1-expressing cells. Dynamic movements of the actin network and talin clusters in protruding regions of GFP-D1-expressing cells were examined in more detail by monitoring talin clusters with GFP-D1. GFP-D1-labeled talin clusters stayed in the same position (Fig. 7*E*, green arrows at *left* of the kymograph; Supplemental Movie S2) but the actin network moved backward over the talin clusters (Fig. 7*E*, red arrows in the kymograph; Supplemental Movie S2). Concomitantly with the backward movement of the actin network, the protrusion velocity of the leading edge was much lower in GFP-D1-expressing cells than that of GFP-expressing cells (Fig. 7*F*). These results support the idea that the talin-vinculin binding is essential to anchor the actin network to FAs and ensures the protrusion of leading edges.

DISCUSSION

In this study, we observed that vinculin delocalized from talin-containing FAs upon actomyosin inhibition and reaccumulated at FAs by stretching the substratum. The accumulation was presumably dependent on the interaction of vinculin with talin. Stress fiber-like structures connected to FAs were necessary for this stretch-dependent vinculin accumulation. On the other hand, talin was retained at FAs in cells in which actomyosin-based force generation was inhibited, and the talin localization was not affected by mechanical forces loaded to FAs by substratum stretching. These results suggest that the tensile force on the actin-talin-integrin linkage is essential for the vinculin accumulation at FAs. This idea is also supported by the findings that talin molecules at FAs are stretched depending on the actomyosin activity in living cells (45), and the amount of vinculin at individual FAs is in proportion to the magnitude of traction forces exerted at the FAs (3). Our IP results (Fig. 6), which showed that the talin-vinculin complex formation was diminished by the expression of the talin-binding domain of vinculin (domain D1), but not its A50I mutant and was augmented under the stretch, suggest that the direct talin-vinculin binding is involved in the force-dependent formation of the talin-vinculin complexes. Future studies using fluorescence resonance energy transfer between talin and vinculin will bring further insights into the dynamic interaction between talin and vinculin in living cells.

Full-length vinculin adopts a globular conformation through the intramolecular interaction between the NH_2-terminal headpiece including the domain D1 and the COOH-terminal tail region (66). In contrast to endogenous, full-length vinculin, GFP-D1 localized at FAs regardless of actomyosin activity (6, 27, this study), and this localization was not affected by stretching of substratum. Interestingly, the head-tail interaction-defective mutant of vinculin, which adopts an extended conformation, also localizes at FAs even in actomyosin-inhibited cells (6). These results imply that the globular conformation of vinculin endows vinculin with the force-dependent talin binding; the domain D1 in globular-shaped vinculin, but not in extended-shaped one, may not gain access to VBSs in talin due to steric constraints unless these sites are fully exposed to a force.

We previously reported that localization of zyxin at FAs is force-dependent; zyxin was delocalized from FAs upon actomyosin inhibition, but the localization at FAs was restored by uniaxial stretching of the substratum, and the localization was dependent on the presence of stress fiber-like structure (25). The localizations of vinculin and zyxin at FAs are regulated distinctively because expression of a dominant negative form of zyxin, which led to the dislocation of zyxin and its binding partner vasodilator-stimulated phosphoprotein from FAs, did not affect vinculin localization at FAs (25). The force-dependent protein assembly at FAs might be regulated independently among proteins.

The talin-mediated link between ECM-bound integrin molecules and the actin cytoskeleton is relatively weak and easily slips (34). Our results suggest the slippage between talin and actin filaments, because talin clusters were retained at FAs in GFP-D1-expressing cells, while the actin network moved backward (Fig. 7*E*). Once a talin molecule associates with the moving actin network, the talin molecule will be stretched between two binding sites for integrin and for the actin filament, and the link will be broken at the actin filament-talin connection when the force exceeds 2 pN (Fig. 8, *A* and *B*). During the association of talin with actin filaments (ca. 5 s) (34), the talin molecule could be stretched by ~300 nm, because the actin cytoskeleton moves at the velocity of 3.8 μm/min as shown in this study. This value agrees with the observation that individual talin molecules in living cells are transiently stretched by 350 nm in the direction of the actin flow (45). The stretched talin molecule will expose multiple VBSs (Fig. 8*B*) (10), which will lead to multiple vinculin bindings to the VBSs. We show here that the vinculin binding to talin is required for anchoring the actin network to talin clusters at FAs in the cell-protruding regions. Since vinculin has an actin-binding site in its COOH-terminal tail region and the talin-binding domain D1 in its NH_2-terminal headpiece

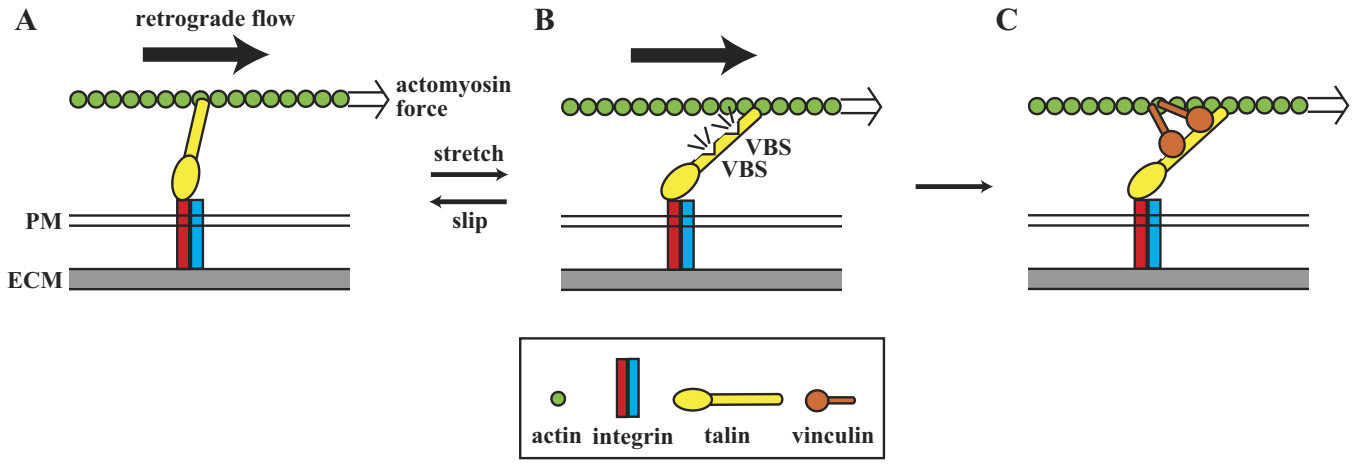

Fig. 8. A model for force-dependent regulation of vinculin recruitment at FAs and anchoring the actin network. *A* and *B*: actomyosin-based force drives retrograde flow of actin filaments. The force stretches talin molecules associated with integrin, and causes exposure of cryptic vinculin-binding sites (VBSs). The actin-talin link slips as the force exceeds ca. 2 pN (*B*). The state (*B*) returns to the state (*A*) when the free actin-binding domain of talin binds again to an actin filament. *C*: vinculin binds to the exposed VBSs via the domain D1 and to the actin filament via its tail domain. See DISCUSSION for more details. ECM, extracellular matrix; PM, plasma membrane.

(66), it can bind to both talin and actin and will strengthen the actin-integrin connection mechanically as illustrated in Fig. 8C. In living cells, each vinculin molecule at adhesion sites is loaded with a mechanical force of ~2.5 pN (22); i.e., the talin-actin link could be reinforced by multiple vinculin molecules and would sustain a much larger force than a simple talin-actin link can do. Consequently, vinculin-bound talin will be maintained in a stretched state (45), contributing to further stabilization of the talin-vinculin bond. This vinculin-reinforced "integrin-talin-vinculin-actin" linkage in parallel with "integrin-talin-actin" one may anchor the actin network (Fig. 8*C*). The anchored actin network would provide a mechanical basis to support the polymerizing actin filaments at the leading edge and ensure the advancement of the leading edge.

The connection between the retrograding actin cytoskeleton and stationary integrin clusters has been modeled as a molecular clutch, where slip between the actin cytoskeleton and integrin is regulated by linker proteins (5, 26, 44). Vinculin has been suggested as a key player in the clutch model (33). According to the clutch model, when the clutch is engaged, the flow of the actin cytoskeleton is slowed down, and polymerizing actin filaments push the leading edge forward (18). Our results suggest that vinculin binding to talin is essential for the clutch engagement, and this binding is regulated by tension in the actin-talin-integrin-ECM link. Our model shown in Fig. 8 agrees with the previous findings: *1*) the linkage between integrin and the actin cytoskeleton is strengthened when this linkage is mechanically loaded (7, 61), *2*) talin is required for the force-induced strengthening of this linkage (17), and *3*) neither the NH_2-terminal nor the COOH-terminal fragment of vinculin alone rescues lamellipodial expansion in vinculin-null cells (63). Recently, Thievessen et al. (58) have reported that the vinculin-actin binding retards the retrograde actin flow and ensures the force transmission from the actin cytoskeleton to ECM, which strongly supports our hypothesis.

Talin and vinculin are important not only for cell adhesions under culture conditions but also for embryonic development. Significance of mechanical regulation in tissue development has also been discussed (31, 48). Vinculin knockout leads to lack of midline fusion of the rostral neural tube (62), and talin knockout causes a failure in gastrulation (46). All these defects arise from improper cell adhesions, actin remodeling, and cell migration (38). Lamellipodia protrusion and traction force exertion at adhesion sites in the lamellipodia are crucial for convergent extension, an essential step in neural tube fusion and gastrulation, in which cells crawl between one another to form a long, narrow array of the cells (60). Force-dependent regulation of the actin-adhesion coupling through talin-vinculin binding would be involved in ensuring lamellipodia protrusion during convergent extension. These points should be examined in future studies.

ACKNOWLEDGMENTS

We thank Cheng-Han Yu and Hiroaki Machiyama for kind gifts of plasmid, Keiko Kawauchi (National University of Singapore) for technical advice, Sri Ram Krishna Vedula (Loreal Research and Innovation) and Yasaman Nematbakhsh (National University of Singapore) for critical reading of the manuscript, and Michael P. Sheetz, Felix Margadant and Xian Hu (National University of Singapore) for helpful discussion.

GRANTS

This work was supported by the Seed Fund from the Mechanobiology Institute at the National University of Singapore, a grant (ICORP/SORST Cell Mechanosensing) from the Japan Science and Technology Agency (to M. Sokabe), and a Grant-in-Aid from the Ministry of Education, Culture, Sports, Science, and Technology, Japan under Grants 15086207, 16GS0308, 21247021, and 24247028 (to M. Sokabe) and 2011009 (to H. Tatsumi).

DISCLOSURES

No conflicts of interest, financial or otherwise, are declared by the author(s).

AUTHOR CONTRIBUTIONS

Author contributions: H.H., H.T., and M.S. conception and design of research; H.H. performed experiments; H.H. and H.T. analyzed data; H.H. interpreted results of experiments; H.H. prepared figures; H.H., H.T., C.T.L., and M.S. drafted manuscript; H.H., H.T., C.T.L., and M.S. approved final version of manuscript.

REFERENCES

1. **Alenghat FJ, Fabry B, Tsai KY, Goldmann WH, Ingber DE.** Analysis of cell mechanics in single vinculin-deficient cells using a magnetic tweezer. *Biochem Biophys Res Commun* 277: 93–99, 2000.
2. **Bakolitsa C, Cohen DM, Bankston LA, Bobkov AA, Cadwell GW, Jennings L, Critchley DR, Craig SW, Liddington RC.** Structural basis for vinculin activation at sites of cell adhesion. *Nature* 430: 583–586, 2004.
3. **Balaban NQ, Schwarz US, Riveline D, Goichberg P, Tzur G, Sabanay I, Mahalu D, Safran S, Bershadsky A, Addadi L, Geiger B.** Force and focal adhesion assembly: a close relationship studied using elastic micropatterned substrates. *Nat Cell Biol* 3: 466–472, 2001.
4. **Bois PR, Borgon RA, Vonrhein C, Izard T.** Structural dynamics of α-actinin-vinculin interactions. *Mol Cell Biol* 25: 6112–6122, 2005.
5. **Brown CM, Hebert B, Kolin DL, Zareno J, Whitmore L, Horwitz AR, Wiseman PW.** Probing the integrin-actin linkage using high-resolution protein velocity mapping. *J Cell Sci* 119: 5204–5214, 2006.
6. **Carisey A, Tsang R, Greiner AM, Nijenhuis N, Heath N, Nazgiewicz A, Kemkemer R, Derby B, Spatz J, Ballestrem C.** Vinculin regulates the recruitment and release of core focal adhesion proteins in a force-dependent manner. *Curr Biol* 23: 271–281, 2013.
7. **Choquet D, Felsenfeld DP, Sheetz MP.** Extracellular matrix rigidity causes strengthening of integrin-cytoskeleton linkages. *Cell* 88: 39–48, 1997.
8. **Conrad PA, Nederlof MA, Herman IM, Taylor DL.** Correlated distribution of actin, myosin, and microtubules at the leading edge of migrating Swiss 3T3 fibroblasts. *Cell Motil Cytoskeleton* 14: 527–543, 1989.
9. **Critchley DR.** Cytoskeletal proteins talin and vinculin in integrin-mediated adhesion. *Biochem Soc Trans* 32: 831–836, 2004.
10. **del Rio A, Perez-Jimenez R, Liu R, Roca-Cusachs P, Fernandez JM, Sheetz MP.** Stretching single talin rod molecules activates vinculin binding. *Science* 323: 638–641, 2009.
11. **Ezzell RM, Goldmann WH, Wang N, Parasharama N, Ingber DE.** Vinculin promotes cell spreading by mechanically coupling integrins to the cytoskeleton. *Exp Cell Res* 231: 14–26, 1997.
12. **Fillingham I, Gingras AR, Papagrigoriou E, Patel B, Emsley J, Critchley DR, Roberts GC, Barsukov IL.** A vinculin binding domain from the talin rod unfolds to form a complex with the vinculin head. *Structure* 13: 65–74, 2005.
13. **Franz CM, Müller DJ.** Analyzing focal adhesion structure by atomic force microscopy. *J Cell Sci* 118: 5315–5323, 2005.
14. **Galbraith CG, Yamada KM, Sheetz MP.** The relationship between force and focal complex development. *J Cell Biol* 159: 695–705, 2002.
15. **Gardel ML, Sabass B, Ji L, Danuser G, Schwarz US, Waterman CM.** Traction stress in focal adhesions correlates biphasically with actin retrograde flow speed. *J Cell Biol* 183: 999–1005, 2008.
16. **Geiger B, Bershadsky A, Pankov R, Yamada KM.** Transmembrane extracellular matrix-cytoskeleton crosstalk. *Nat Rev Mol Cell Biol* 2: 793–805, 2001.
17. **Giannone G, Jiang G, Sutton DH, Critchley DR, Sheetz MP.** Talin1 is critical for force-dependent reinforcement of initial integrin-cytoskeleton bonds but not tyrosine kinase activation. *J Cell Biol* 163: 409–419, 2003.
18. **Giannone G, Mège RM, Thoumine O.** Multi-level molecular clutches in motile cell processes. *Trends Cell Biol* 19: 475–486, 2009.

19. **Gilmore AP, Jackson P, Waites GT, Critchley DR.** Further characterisation of the talin-binding site in the cytoskeletal protein vinculin. *J Cell Sci* 103: 719–731, 1992.
20. **Gingras AR, Ziegler WH, Frank R, Barsukov IL, Roberts GC, Critchley DR, Emsley J.** Mapping and consensus sequence identification for multiple vinculin binding sites within the talin rod. *J Biol Chem* 280: 37217–37224, 2005.
21. **Goeckeler ZM, Bridgman PC, Wysolmerski RB.** Nonmuscle myosin II is responsible for maintaining endothelial cell basal tone and stress fiber integrity. *Am J Physiol Cell Physiol* 295: C994–C1006, 2008.
22. **Grashoff C, Hoffman BD, Brenner MD, Zhou R, Parsons M, Yang MT, McLean MA, Sligar SG, Chen CS, Ha T, Schwartz MA.** Measuring mechanical tension across vinculin reveals regulation of focal adhesion dynamics. *Nature* 466: 263–266, 2010.
23. **Hayakawa K, Tatsumi H, Sokabe M.** Actin stress fibers transmit and focus force to activate mechanosensitive channels. *J Cell Sci* 121: 496–503, 2008.
24. **Hirata H, Lim CT, Miyata H.** 3D coupling of fibronectin fibril arrangement with topology of ventral plasma membrane. *Cell Commun Adhes* 19: 17–23, 2012.
25. **Hirata H, Tatsumi H, Sokabe M.** Mechanical forces facilitate actin polymerization at focal adhesions in a zyxin-dependent manner. *J Cell Sci* 121: 2795–2804, 2008.
26. **Hu K, Ji L, Applegate KT, Danuser G, Waterman-Storer CM.** Differential transmission of actin motion within focal adhesions. *Science* 315: 111–115, 2007.
27. **Humphries JD, Wang P, Streuli C, Geiger B, Humphries MJ, Ballestrem C.** Vinculin controls focal adhesion formation by direct interactions with talin and actin. *J Cell Biol* 179: 1043–1057, 2007.
28. **Hüttelmaier S, Mayboroda O, Harbeck B, Jarchau T, Jockusch BM, Rüdiger M.** The interaction of the cell-contact proteins VASP and vinculin is regulated by phosphatidylinositol-4,5-bisphosphate. *Curr Biol* 8: 479–488, 1998.
29. **Hytönen VP, Vogel V.** How force might activate talin's vinculin binding sites: SMD reveals a structural mechanism. *PLoS Comput Biol* 4: e24, 2008.
30. **Ingber DE.** Cellular mechanotransduction: putting all the pieces together again. *FASEB J* 20: 811–827, 2006.
31. **Ingber DE.** Mechanical control of tissue morphogenesis during embryological development. *Int J Dev Biol* 50: 255–266, 2006.
32. **Izard T, Evans G, Borgon RA, Rush CL, Bricogne G, Bois PR.** Vinculin activation by talin through helical bundle conversion. *Nature* 427: 171–175, 2004.
33. **Ji L, Lim J, Danuser G.** Fluctuations of intracellular forces during cell protrusion. *Nat Cell Biol* 10: 1393–1400, 2008.
34. **Jiang G, Giannone G, Critchley DR, Fukumoto E, Sheetz MP.** Two-piconewton slip bond between fibronectin and the cytoskeleton depends on talin. *Nature* 424: 334–337, 2003.
35. **Katz BZ, Zamir E, Bershadsky A, Kam Z, Yamada KM, Geiger B.** Physical state of the extracellular matrix regulates the structure and molecular composition of cell-matrix adhesions. *Mol Biol Cell* 11: 1047–1060, 2000.
36. **Kelly DF, Taylor DW, Bakolitsa C, Bobkov AA, Bankston L, Liddington RC, Taylor KA.** Structure of the α-actinin-vinculin head domain complex determined by cryo-electron microscopy. *J Mol Biol* 357: 562–573, 2006.
37. **Kiyoshima D, Kawakami K, Hayakawa K, Tatsumi H, Sokabe M.** Force- and Ca^{2+}-dependent internalization of integrins in cultured endothelial cells. *J Cell Sci* 124: 3859–3870, 2011.
38. **Köhler A, Schambony A, Wedlich D.** Cell migration under control of Wnt-signaling in the vertebrate embryo. In: *Wnt Signaling in Embryonic Development*, edited by Sokol SY. San Diego, CA: Elsevier, 2007.
39. **Kumar S, Maxwell IZ, Heisterkamp A, Polte TR, Lele TP, Salanga M, Mazur E, Ingber DE.** Viscoelastic retraction of single living stress fibers and its impact on cell shape, cytoskeletal organization, and extracellular matrix mechanics. *Biophys J* 90: 3762–3773, 2006.
40. **Kuo JC, Han X, Hsiao CT, Yates JR 3rd, Waterman CM.** Analysis of the myosin-II-responsive focal adhesion proteome reveals a role for β-Pix in negative regulation of focal adhesion maturation. *Nat Cell Biol* 13: 383–393, 2011.
41. **Kuroda S, Fukata M, Nakagawa M, Fujii K, Nakamura T, Ookubo T, Izawa I, Nagase T, Nomura N, Tani H, Shoji I, Matsuura Y, Yonehara S, Kaibuchi K.** Role of IQGAP1, a target of the small GTPases Cdc42 and Rac1, in regulation of E-cadherin-mediated cell-cell adhesion. *Science* 281: 832–835, 1998.
42. **Lee SE, Roger D, Kamm RD, Mofrad MR.** Force-induced activation of talin and its possible role in focal adhesion mechanotransduction. *J Biomech* 40: 2096–2106, 2007.
43. **Lele TP, Pendse J, Kumar S, Salanga M, Karavitis J, Ingber DE.** Mechanical forces alter zyxin unbinding kinetics within focal adhesions of living cells. *J Cell Physiol* 207: 187–194, 2006.
44. **Lin CH, Forscher P.** Growth cone advance is inversely proportional to retrograde F-actin Flow. *Neuron* 14: 763–771, 1995.
45. **Margadant F, Chew LL, Hu X, Yu H, Bate N, Zhang X, Sheetz M.** Mechanotransduction in vivo by repeated talin stretch-relaxation events depends upon vinculin. *PLoS Biol* 9: e1001223, 2011.
46. **Monkley SJ, Zhou XH, Kinston SJ, Giblett SM, Hemmings L, Priddle H, Brown JE, Pritchard CA, Critchley DR, Fässler R.** Disruption of the talin gene arrests mouse development at the gastrulation stage. *Dev Dyn* 219: 560–574, 2000.
47. **Moore SW, Roca-Cusachs P, Sheetz MP.** Stretchy proteins on stretchy substrates: the important elements of integrin-mediated rigidity sensing. *Dev Cell* 19: 194–206, 2010.
48. **Nelson CM, Gleghorn JP.** Sculpting organs: mechanical regulation of tissue development. *Annu Rev Biomed Eng* 14: 129–154, 2012.
49. **Papagrigoriou E, Gingras AR, Barsukov IL, Bate N, Fillingham IJ, Patel B, Frank R, Ziegler WH, Roberts GC, Critchley DR, Emsley J.** Activation of a vinculin-binding site in the talin rod involves rearrangement of a five-helix bundle. *EMBO J* 23: 2942–2951, 2004.
50. **Pasapera AM, Schneider IC, Rericha E, Schlaepfer DD, Waterman CM.** Myosin II activity regulates vinculin recruitment to focal adhesions through FAK-mediated paxillin phosphorylation. *J Cell Biol* 188: 877–890, 2010.
51. **Patel B, Gingras AR, Bobkov AA, Fujimoto LM, Zhang M, Liddington RC, Mazzeo D, Emsley J, Roberts GC, Barsukov IL, Critchley DR.** The activity of the vinculin binding sites in talin is influenced by the stability of the helical bundles that make up the talin rod. *J Biol Chem* 281: 7458–7467, 2006.
52. **Patel I, Volberg T, Elad N, Hirschfeld-Warneken V, Grashoff C, Fässler R, Spatz JP, Geiger B, Medalia O.** Dissecting the molecular architecture of integrin adhesion sites by cryo-electon tomography. *Nat Cell Biol* 12: 909–915, 2010.
53. **Pavalko FM, Burridge K.** Disruption of the cytoskeleton after microinjection of proteolytic fragments of α-actinin. *J Cell Biol* 114: 481–491, 1991.
54. **Rajfur Z, Roy P, Otey C, Romer L, Jacobson K.** Dissecting the link between stress fibers and focal adhesions by CALI with EGFP fusion proteins. *Nat Cell Biol* 4: 286–293, 2002.
55. **Riveline D, Zamir E, Balaban NQ, Schwarz US, Ishizaki T, Narumiya S, Kam Z, Geiger B, Bershadsky AD.** Focal contacts as mechanosensors: externally applied local mechanical force induces growth of focal contacts by an mDia1-dependent and ROCK-independent mechanism. *J Cell Biol* 153: 1175–1185, 2001.
56. **Smith AL, Friedman DB, Yu H, Carnahan RH, Reynolds AB.** ReCLIP (reversible cross-link immuno-precipitation): an efficient method for interrogation of labile protein complexes. *PLoS One* 6: e16206, 2011.
57. **Straight AF, Cheung A, Limouze J, Chen I, Westwood NJ, Sellers JR, Mitchison TJ.** Dissecting temporal and spatial control of cytokinesis with a myosin II inhibitor. *Science* 299: 1743–1747, 2003.
58. **Thievessen I, Thompson PM, Berlemont S, Plevock KM, Plotnikov SV, Zemljic-Harpf A, Ross RS, Davidson MW, Danuser G, Campbell SL, Waterman CM.** Vinculin-actin interaction couples actin retrograde flow to focal adhesions, but is dispensable for focal adhesion growth. *J Cell Biol* 202: 163–177, 2013.
59. **Uehata M, Ishizaki T, Satoh H, Ono T, Kawahara T, Morishita T, Tamakawa H, Yamagami K, Inui J, Maekawa M, Narumiya S.** Calcium sensitization of smooth muscle mediated by a Rho-associated protein kinase in hypertension. *Nature* 389: 990–994, 1997.
60. **Wallingford JB, Fraser SE, Harland RM.** Convergent extension: the molecular control of polarized cell movement during embryonic development. *Dev Cell* 2: 695–706, 2002.
61. **Wang N, Butler JP, Ingber DE.** Mechanotransduction across the cell surface and through the cytoskeleton. *Science* 260: 1124–1127, 1993.

62. **Xu W, Baribault H, Adamson ED.** Vinculin knockout results in heart and brain defects during embryonic development. *Development* 125: 327–337, 1998.
63. **Xu W, Coll JL, Adamson ED.** Rescue of the mutant phenotype by reexpression of full-length vinculin in null F9 cells; effects on cell locomotion by domain deleted vinculin. *J Cell Sci* 111: 1535–1544, 1998.
64. **Yu CH, Law JB, Suryana M, Low HY, Sheetz MP.** Early integrin binding to Arg-Gly-Asp peptide activates actin polymerization and contractile movement that stimulates outward translocation. *Proc Natl Acad Sci USA* 108: 20585–20590, 2011.
65. **Zhang X, Jiang G, Cai Y, Monkley SJ, Critchley DR, Sheetz MP.** Talin depletion reveals independence of initial cell spreading from integrin activation and traction. *Nat Cell Biol* 10: 1062–1068, 2008.
66. **Ziegler WH, Liddington RC, Critchley DR.** The structure and regulation of vinculin. *Trends Cell Biol* 16: 453–460, 2006.